Impacts of midlatitude precursor emissions and local photochemistry on ozone abundances in the Arctic

T. W. Walker,[1] D. B. A. Jones,[1] M. Parrington,[1,2] D. K. Henze,[3] L. T. Murray,[4] J. W. Bottenheim,[5] K. Anlauf,[5] J. R. Worden,[6] K. W. Bowman,[6] C. Shim,[7] K. Singh,[8] M. Kopacz,[9] D. W. Tarasick,[5] J. Davies,[5] P. von der Gathen,[10] A. M. Thompson,[11] and C. C. Carouge[4]

[1] We assess the impact of transport of pollution from midlatitudes on the abundance of ozone in the Arctic in summer 2006 using the GEOS-Chem global chemical transport model and its adjoint. We find that although the impact of midlatitude emissions on ozone abundances in the Arctic is at a maximum in fall and winter, in July transport from North America, Asia, and Europe together contributed about 25% of surface ozone abundances in the Arctic. Throughout the summer, the dominant source of ozone in the Arctic troposphere was photochemical production within the Arctic, which accounted for more than 50% of the ozone in the Arctic boundary layer and as much as 30%–40% of the ozone in the middle troposphere. An adjoint sensitivity analysis of the impact of NO_x emissions on ozone at Alert shows that on synoptic time scales in both the lower and middle troposphere, ozone abundances are more sensitive to emissions between 50°N and 70°N, with important influences from anthropogenic, biomass burning, soil, and lightning sources. Although local surface NO_x emissions contribute to ozone formation, transport of NO_x in the form of peroxyacetyl nitrate (PAN) from outside the Arctic and from the upper troposphere also contributed to ozone production in the lower troposphere. We find that in late May and June the release of NO_x from PAN decomposition accounted for 93% and 55% of ozone production at the Arctic surface, respectively.

Citation: Walker, T. W., et al. (2012), Impacts of midlatitude precursor emissions and local photochemistry on ozone abundances in the Arctic, *J. Geophys. Res.*, *117*, D01305, doi:10.1029/2011JD016370.

1. Introduction

[2] The Arctic contains a fragile ecosystem that is expected to be sensitive to changes in climate and to transported air pollution from midlatitudes [*Law and Stohl*, 2007;

[1]Department of Physics, University of Toronto, Toronto, Ontario, Canada.
[2]School of Geosciences, University of Edinburgh, Edinburgh, UK.
[3]Department of Mechanical Engineering, University of Colorado at Boulder, Boulder, Colorado, USA.
[4]School of Engineering and Applied Sciences, Harvard University, Cambridge, Massachusetts, USA.
[5]Environment Canada, Downsview, Ontario, Canada.
[6]Jet Propulsion Laboratory, California Institute of Technology, Pasadena, California, USA.
[7]Korea Environment Institute, Seoul, South Korea.
[8]Department of Computer Science, Virginia Polytechnic Institute and State University, Blacksburg, Virginia, USA.
[9]Woodrow Wilson School of Public and International Affairs, Princeton University, Princeton, New Jersey, USA.
[10]Research Unit Potsdam, Alfred Wegener Institute for Polar and Marine Research, Potsdam, Germany.
[11]Department of Meteorology, Pennsylvania State University, University Park, Pennsylvania, USA.

Jacobson, 2010]. Tropospheric ozone, which is both a greenhouse gas and an air contaminant with adverse effects on the health of humans and other biota, is therefore of critical importance. Despite the paucity of local sources of O_3 precursors such as nitrogen oxides ($NO_x = NO + NO_2$), the Arctic troposphere at times has large concentrations of O_3, which exhibit a strong seasonality. This seasonality, including a springtime maximum in the free troposphere, is poorly understood [*Monks*, 2000; *Law and Stohl*, 2007] and reflects a combination of local production, stratospheric influence, and transport from a variety of midlatitude sources of precursors, including emissions from combustion at the surface and from lightning in the upper troposphere.

[3] Modeling studies on transport into the Arctic have traditionally focused on passive tracers [*Eckhardt et al.*, 2003], carbon monoxide [*Klonecki et al.*, 2003; *Lamarque and Hess*, 2003; *Duncan and Bey*, 2004], and aerosols [*Koch and Hansen*, 2005; *Stohl*, 2006]. Recent work by *Shindell et al.* [2008] presented a multimodel analysis of ozone and other gaseous species but did not elaborate on the source of precursor emissions, whether anthropogenic, biomass burning, or lightning. Study of the loading of the Arctic troposphere with reactive nitrogen ($NO_y = NO_x$ + peroxyacetyl nitrate (PAN) + methacryloyl peroxy nitrate

(MPAN) + peroxy propionyl nitrate (PPN) + NO_3 + $2N_2O_5$ + HNO_4 + HNO_3) species and their impacts on local ozone production is also lacking [*Quinn et al.*, 2008]. The spring maximum in high-latitude tropospheric ozone and the summertime budget of ozone production are not well understood [*Law and Stohl*, 2007] and the impact of midlatitude surface emissions on Arctic pollutant abundances is contentious [*Koch and Hansen*, 2005; *Stohl*, 2006; *Hirdman et al.*, 2010].

[4] Trends in the Arctic over the past decade show that tropospheric ozone is increasing [*Oltmans et al.*, 2006; *Helmig et al.*, 2007; *Kivi et al.*, 2007], although changes on decadal time scales may be related to changes in the lower stratosphere [*Tarasick et al.*, 2005], or the phase of either the North Atlantic Oscillation [*Eckhardt et al.*, 2003] or the Arctic Oscillation [*Kivi et al.*, 2007]. Particulate nitrate concentrations at the surface, which correlate with peroxyacetyl nitrate (PAN) concentrations in the Arctic, also exhibit an increasing trend over time [*Quinn et al.*, 2007].

[5] Previous studies have found that the sensitivity of the Arctic surface to midlatitude anthropogenic emissions is largest in winter and spring, with Eurasian sources being the dominant influence [*Klonecki et al.*, 2003; *Eckhardt et al.*, 2003; *Wang et al.*, 2003; *Duncan and Bey*, 2004]. More recent work by *Shindell et al.* [2008] further indicates that in the Arctic midtroposphere, ozone abundances are most sensitive to transport from midlatitudes in spring and summer, with an important contribution from East Asia. Transport from the stratosphere into the Arctic troposphere also peaks in spring, which can provide both ozone and NO_x to the upper troposphere [*Liang et al.*, 2009].

[6] Lightning NO_x emissions are a large uncertainty in the global NO_x budget, with estimates ranging from 2 to 8 Tg N yr^{-1} [*Schumann and Huntrieser*, 2007]. The midlatitude to tropical partitioning of the source is also unclear [*Huntrieser et al.*, 2008]. Remote sensing observations of global lightning flash distributions can provide improved spatial distributions of lightning NO_x emissions [*Sauvage et al.*, 2007; *Walker et al.*, 2010]. Furthermore, satellite observations of O_3 in the free troposphere when assimilated into a chemical transport model provide a valuable constraint on the background ozone distribution resulting in part from lightning emissions [*Martin et al.*, 2007; *Parrington et al.*, 2008, 2009].

[7] While NO_x has a short atmospheric lifetime in the lower troposphere that limits its effect on ozone production to an area near to its emissions source, partitioning into long-lived reservoirs of reactive nitrogen such as peroxyacetyl nitrate (PAN) and its structural analogues permits midlatitude NO_x emissions to effect ozone production far from their sources [*Singh*, 1987]. PAN is long-lived at low temperatures, and acts to redistribute the ozone producing capacity of NO_x to areas where NO_x emissions may be small [*Moxim et al.*, 1996; *Levy et al.*, 1999; *Walker et al.*, 2010]. PAN is the dominant species in the high-latitude budget of reactive nitrogen [*Singh et al.*, 1992; *Bottenheim et al.*, 1993; *Talbot et al.*, 1994]. *Beine and Krojnes* [2000] find that most PAN decomposition in the Arctic occurs during the summer, and this releases a significant amount of NO_x that enhances ozone production [*Fan et al.*, 1994]. However, the effects of this decomposition on ozone production has not yet been quantified over the course of a full season.

[8] We employ the GEOS-Chem global chemical transport model (CTM) to quantify the budget of tropospheric ozone in the Arctic in summer. In particular, we are interested in understanding the impact of long-range transport of PAN on ozone abundances in the Arctic. We exploit satellite observations of tropospheric ozone from the Tropospheric Emission Spectrometer (TES) to provide an improved description of midlatitude ozone abundances in the model to better assess the fidelity of the model simulation of transport into the Arctic. We also use the adjoint of the GEOS-Chem model to characterize the sensitivity of ozone abundances in the Arctic to precursor emissions at middle and high latitudes throughout spring and summer. We focus on summer 2006 because previous studies [e.g., *Parrington et al.*, 2008; *Zhang et al.*, 2008; *Walker et al.*, 2010] have evaluated the GEOS-Chem midlatitude simulation for this period using TES data and aircraft observations. We also take advantage of surface observations of PAN at Alert in 2001 to evaluate the model simulation of PAN.

[9] We begin in section 2 with a description of the observational data and modeling tools used in this study. In section 3 we use observations from the TES instrument to assess the fidelity of the modeled transport into the Arctic and then present an analysis of the impact of transport of ozone from midlatitude continental source regions on the Arctic ozone budget. In section 4 we quantify the impact of reactive nitrogen on ozone production in the Arctic troposphere. Finally, in section 5 we conduct a detailed sensitivity analysis of ozone in the Arctic to particular precursor NO_x emissions at middle and high latitudes.

2. Observations and Modeling

2.1. Surface Observations

[10] We employ surface observations of ozone and PAN from a high-latitude site at Alert, Canada (82°N, 62°W) to evaluate model performance. Measurements of ozone were reported as hourly average mixing ratio from a commercial instrument based on UV absorption [*Bottenheim et al.*, 2002]. PAN measurements are recorded every half hour with a gas chromatograph instrument with electron capture detection [*Bottenheim et al.*, 1993].

[11] Figure 1 shows the daily average ozone values as measured at the Alert station throughout 2001 (in black). Ozone accumulates during winter in the absence of photochemically driven loss processes, reaching maximum concentrations in spring. In the spring, concentrations episodically decrease rapidly to very low values as a result of rapid ozone depletions at the surface, linked to bromine radical chemistry [*Fan and Jacob*, 1992; *Bottenheim et al.*, 2002, 2009]. In early summer surface ozone concentrations decrease and remain low throughout the summer.

2.2. Ozonesondes

[12] Ozonesonde data from the World Ozone and Ultraviolet Radiation Data Centre (WOUDC) provide a source of independent observations of free tropospheric ozone. Data from high-latitude sites at Eureka, Canada (80°N, 86°W) and Ny-Ålesund, Norway (79°N, 12°E) from 2005 and 2006 are used to validate the simulated ozone field and gauge improvements in model performance (World Ozone and
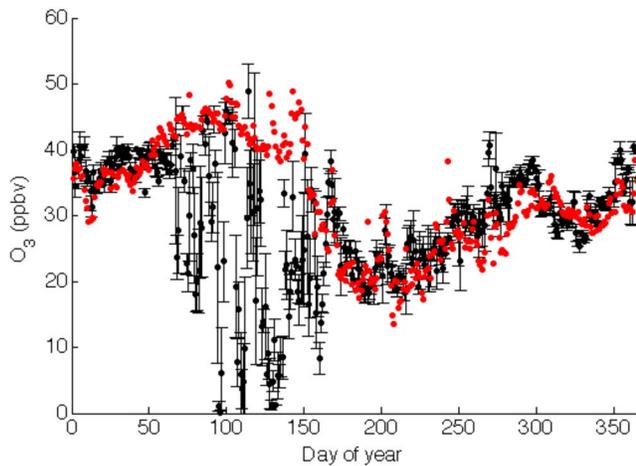
Figure 1. Seasonal cycle of ozone at the surface at Alert (82°N, 62°W) in 2001. Red symbols indicate simulated values from the baseline simulation; black symbols are daily average values of the observations. Vertical error bars represent the standard deviation in the observations over the course of the day.

Ultraviolet Radiation Centre (WOUDC), retrieved on 10 December 2009 from http://www.woudc.org/.) Launches of electrochemical cell (ECC) sondes at these sites were roughly weekly at Eureka and Ny-Ålesund, except at Eureka during the Canadian Arctic Atmospheric Chemistry Experiment (ACE) Validation Campaign around polar sunrise and

at Ny-Ålesund during stratospheric ozone loss campaigns (e.g., Match) during winter when launches during both periods were more frequent.

[13] One year of observations in 2005 are shown in Figure 2 (top). Eureka launched 67 sondes and Ny-Ålesund launched 82 in 2005. The ozone values are averaged into monthly bins here. Ozone depletion near the surface also appears in the Eureka sonde record in April where moderately low surface values (<30 ppbv) persist until autumn, but in the middle and upper troposphere ozone concentrations peak in the spring. Ozone concentrations remain high at these altitudes through the summer and reach a minimum in winter.

2.3. Tropospheric Emission Spectrometer

[14] The TES instrument [*Beer et al.*, 2001] is a high-resolution infrared Fourier spectrometer on board NASA's Aura satellite. The Aura satellite was launched in July 2004 into a Sun-synchronous polar orbit with a local equator crossing time of 13:45 and a repeat cycle of 16 days. The instrument observes in the nadir at wavelengths from 650 to 3050 cm^{-1} with an apodized spectral resolution of 0.1 cm^{-1}. TES currently operates in global survey mode, taking observations every 220 km along track with an instrument field of view of 8 km $\times$ 5 km at the surface.

[15] Ozone profiles are retrieved from TES radiances using an optimal estimation approach [*Bowman et al.*, 2002, 2006; *Worden et al.*, 2004]. Ozone abundances are expressed as the natural logarithm of the volume mixing ratio in the retrievals, which are performed on a 67-level vertical grid
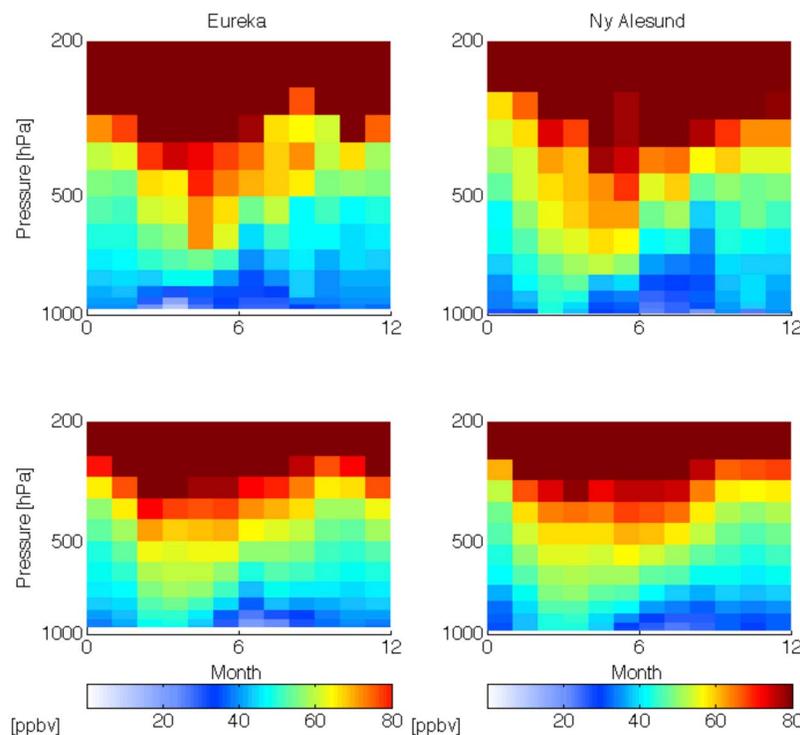

Figure 2. Seasonal cycle of ozone profiles above (left) Eureka (80°N, 86°W and (right) Ny-Ålesund (79°N, 12°E) in 2005. (top) World Ozone and Ultraviolet Radiation Data Centre (WOUDC) ozonesonde data (67 soundings at Eureka and 82 at Ny-Ålesund). (bottom) The monthly ozone values at this location from the baseline simulation (v8-01-04) in GEOS-Chem.

Table 1. Description of Simulations Performed With the GEOS-Chem Model

Simulation	Version	Description
Baseline	v8-01-04	Lightning NO_x emissions use regional OTD-LIS scaling. Surface emissions from EDGAR are overwritten by recent regional emission inventories (EMEP, Streets 2006, NEI99, CAC, BRAVO). Biomass burning emissions from GFED2.
Old emissions	v8-01-04	Lightning NO_x emissions use regional OTD-LIS scaling. Surface emissions from GEIA are overwritten with NEI99. Biomass burning emissions from *Duncan et al.* [2003].
No PAN	v8-01-04	Same emissions as baseline run, but with conversion between NO_x and PAN turned off.
TES assimilation	v7-02-04	Lightning NO_x emissions are not scaled to OTD-LIS. Surface emissions from GEIA are overwritten with NEI99. Biomass burning emissions from *Duncan et al.* [2003]. Assimilation of TES O_3 and CO profiles equatorward of 60° latitude.
Assimilation control	v7-02-04	Same emissions as assimilation run, but with assimilation turned off.
Tagged Ox	v8-01-04	Same emissions as baseline run.

with spacing of approximately 1 km. On average, TES ozone retrievals contain between 3 and 4 degrees of freedom for signal, fewer than 1.5 of which are contributed by the troposphere in extratropical retrievals. TES ozone retrievals have been validated with sonde data [*Worden et al.*, 2007; *Nassar et al.*, 2008; *Boxe et al.*, 2010] and lidar data [*Richards et al.*, 2008] and show a 10%–15% bias in the free troposphere. Retrieved TES ozone and carbon monoxide profiles from July to August 2006 are incorporated into the analysis through the assimilation process described in section 2.4.

2.4. GEOS-Chem Chemical Transport Model

[16] We use the GEOS-Chem global chemical transport model (http://www.geos-chem.org/). The model is driven by assimilated meteorological fields from the Goddard Earth Observing System (GEOS-4) from the NASA Global Modeling and Assimilation Office. The fields have a spatial resolution of 1° × 1.25° with 55 vertical levels, but they are degraded to the CTM resolution of 4° × 5°. The model includes a detailed NO_x–O_x–hydrocarbon chemical mechanism which was first described by *Bey et al.* [2001], with updates by several recent studies [e.g., *Fiore et al.*, 2002; *Martin et al.*, 2002, 2003; *Evans and Jacob*, 2005]. The stratospheric source of ozone is represented by the linearized ozone (LINOZ) parametrization by *McLinden et al.* [2000]. Emissions of lightning NO_x are initially estimated according to *Price and Rind* [1992], with the vertical distribution prescribed by *Pickering et al.* [1998]. Anthropogenic emissions are based on the Global Emissions Inventory Activity (GEIA) [*Benkovitz et al.*, 1996] and overwritten with updated regional inventories where available.

[17] In this study, we use versions v7-02-04 and v8-01-04 of GEOS-Chem; v8-01-04 is used for our baseline simulation and for much of the analysis presented here, whereas v7-02-04 is used for the assimilation of the TES data. Version v8-01-04 corrects a problem with excessive stratosphere-troposphere exchange near the polar tropopause. Version v8-01-04 also incorporates a significant improvement to the global horizontal distribution of lightning NO_x emissions, in which estimated distribution of lightning flashes is scaled to resemble that observed by the Optical Transient Detector and Lightning Imaging Sensor (OTD-LIS) in a method similar to that employed by *Sauvage et al.* [2007].

[18] The two model versions also have significant differences in their anthropogenic and biomass burning emissions inventories. Anthropogenic emissions in v7-02-04 of GEOS-

Chem use the GEIA inventory. GEIA is overwritten in the United States by the Environmental Protection Agency National Emission Inventory (EPA/NEI99), modified according to *Hudman et al.* [2007]. Global anthropogenic emissions are scaled to the simulation year or as far as 1998 according to fuel consumption statistics [*Bey et al.*, 2001]. Biomass burning emissions are monthly averages derived from a four year climatology of remote sensing data [*Duncan et al.*, 2003]. A summary of the differences in the precursor emissions between the two models is given in Table 1.

[19] In v8-01-04, global anthropogenic emissions are from the Emission Database for Global Atmospheric Research (EDGAR, v3.2 [*Olivier and Berdowski*, 2001]) for NO_x, CO, and SO_2. The global inventory is overwritten by regional inventories over the United States (EPA/NEI99 with modifications by *Hudman et al.* [2007]), Europe (EMEP [*Vestreng and Klein*, 2002]), East Asia (Streets [*Streets et al.*, 2003, 2006]), Mexico (BRAVO [*Kuhns et al.*, 2005]), and Canada (CAC, Environment Canada; see http://www.ec.gc.ca/pdb/cac/cac_home_e.cfm). Global emissions are scaled forward to the simulation year or as far as 2005 according to more recent fuel consumption statistics [*van Donkelaar et al.*, 2008]. Biomass burning emissions in v8-01-04 use the GFED2 emissions inventory [*van der Werf et al.*, 2006]. Simulations in this study use emissions and meteorology specific to the year the observations to which we are comparing were taken. Table 2 shows the total NO_x, CO, and volatile organic carbon (VOC) emissions for 2006.

[20] Version v8-01-04 of GEOS-Chem (the baseline simulation) reproduces well many of the observed features of the Arctic ozone distribution. Figure 1 compares a year of ozone mixing ratios at Alert in 2001 to the daily averaged modeled values. Error bars represent the standard deviation of the hourly measurements and capture the variability over the course of each day. GEOS-Chem simulates well the seasonal cycle of ozone, capturing the buildup of concentrations throughout winter as well as the summer minimum. In the spring, observations of ozone fall to low values as a result of rapid ozone loss at the surface because of the previously mentioned catalytic destruction by bromine radicals [*Fan and Jacob*, 1992; *Bottenheim et al.*, 2002, 2009]. The version of GEOS-Chem used in this study does not include these bromine reactions in its chemical mechanism, and thus the model does not capture the low ozone values in spring. Excluding the springtime ozone observations yields a model bias relative to the ozone measurements of −1.1 ppbv (−4%). Figure 2 shows a comparison between the model and ozonesonde measurements above Eureka and

Table 2. Emissions From Anthropogenic Source Inventories Used in GEOS-Chem[a]

Inventory	Domain	Total NO_x (Tg N/yr)	Total CO (Tg C/yr)	Total VOC (Tg C/yr)
Old emissions (GEIA)	Global	24.0	142.2	47.4
Baseline (EDGAR)	Global	27.1	188.3	48.2
EPA/NEI99	United States	−1.2	−1.8	−0.3
CAC	Canada	+0.1	−0.4	−0.3
BRAVO	Mexico	−0.1	−0.4	−0.1
EMEP	Europe	+0.5	−12.4	−5.0
Streets	East Asia	+3.1	+56.7	+4.5

[a]The old emissions and baseline rows give global total anthropogenic NO_x, CO, and volatile organic carbon (VOC) emissions from those simulations, including any regional inventories used. Regional inventories overwrite the global inventories as described in the text. Changes in regional emissions are shown relative to the old emissions simulation. A negative change indicates that emissions are lower in the baseline simulation. Values are based on emissions from April applied throughout the entire year.

Ny-Ålesund in 2005. Although the focus of our analysis in of summer 2006, we compare the model simulation here with ozonesonde data from Eureka and Ny-Ålesund in 2005 because the more complete data record at Ny-Ålesund in 2005 enables us to better examine the model simulation over the seasonal cycle. The model captures the free tropospheric maximum in the spring, but the maximum occurs earlier in spring and is broader in the model. In summer the model slightly underestimates the ozone abundances in the mid-troposphere, with mean summertime biases around 500 hPa of 11% above Eureka and 5% above Ny-Ålesund. In section 3.2 we examine the seasonal dependence of the impact of the midlatitude source regions on ozone at Eureka and Ny-Ålesund.

2.5. Adjoint Model of GEOS-Chem

[21] The adjoint of the GEOS-Chem model was initially described by *Henze et al.* [2007], and is based on GEOS-Chem version v8-02-01. The adjoint model is a computationally efficient tool that calculates the gradient of model outputs (e.g., metrics of species concentrations) to all model inputs (e.g., emissions) around the model state. The gradients may be used together with observations in variational data assimilation, or in inverse modeling to determine the relative change required in the model inputs to effect a desired output state. The GEOS-Chem adjoint was initially developed for inverse modeling of aerosol precursors [*Henze et al.*, 2007, 2009]. It has since been applied for inverse modeling of CO [*Kopacz et al.*, 2009, 2010] and tropospheric ozone [*Zhang et al.*, 2009]. Most recently it has been used for assimilation of space-based tropospheric ozone observations from the TES instrument [*Singh et al.*, 2010]. Most components of the GEOS-Chem adjoint model are derived using automatic differentiation algorithms [*Giering and Kaminski*, 1998; *Sandu et al.*, 2003; *Daescu et al.*, 2003]. The adjoint of the advection operator uses a continuous approach, where the same advection scheme is solved as in the forward model, but the winds are reversed, an approach favored over discrete differentiation for the type of advection scheme employed in GEOS-Chem [*Henze et al.*, 2007; *Hakami et al.*, 2007; *Gou and Sandu*, 2011].

[22] We perform a set of adjoint simulations to probe the sensitivity of ozone concentrations above Alert to emissions of NO_x from various sources. Simulations are performed to calculate sensitivities of both the lower (surface to 850 hPa) and middle (850 to 500 hPa) troposphere above Alert in the first two weeks of each month from April to August, 2006. The resulting sensitivities represent the fractional change in the ozone concentration above Alert due to a unit change in the emissions in each model grid box.

3. Results and Discussion

3.1. Evaluation of Transport of Ozone Into the Arctic in GEOS-Chem

[23] We assimilate TES ozone data into GEOS-Chem to evaluate the model simulation of ozone transport into the Arctic. The assimilation system is described by *Parrington et al.* [2008]. It is based on version v7-02-04 of GEOS-Chem and employs a suboptimal sequential Kalman filter which ingests the TES profiles of tropospheric ozone in a 6 h analysis cycle along the TES orbit track. We assimilate TES data for July and August 2006, equatorward of 60°N. The bias in the TES data, as estimated by *Nassar et al.* [2008], was removed before assimilation of the data. As described by *Parrington et al.* [2008], the initial forecast error is taken as 50% of the initial forecast field and horizontal correlations in the forecast error covariance matrix are neglected. The analysis increment above 100 hPa is set to zero so as to constrain only tropospheric O_3. As shown in Figure 3, the assimilation significantly increases the ozone abundance throughout the free troposphere in the extratropics, compared to the control run without TES assimilation (referred to as the "assimilation control"). *Parrington et al.* [2008] showed that over North America the assimilation reduced the model bias relative to ozonesondes from 10%–25% to less than 5% between 300 and 800 hPa. The TES assimilation was also evaluated by *Worden et al.* [2009] over North Africa, the Middle East, and Asia. They compared the TES assimilation in GEOS-Chem with assimilated ozone data from the Microwave Limb Sounder (MLS) and the Ozone Monitoring Instrument (OMI) in the GEOS-4 data assimilation system at NASA GMAO. They found that assimilation of TES data into GEOS-Chem reduced the bias in the model relative to the OMI and MLS assimilated fields at GMAO from 6.8 ppbv to 1.4 ppbv in the upper troposphere across the region, suggesting that the TES assimilation provided an improved description of tropospheric ozone in the model, that is consistent with the information from the OMI and MLS satellite instruments. Since the TES assimilation strongly constrains the distribution of midlatitude ozone, we can validate the meridional transport into the Arctic in the model by assimilating TES data outside the Arctic to provide a midlatitude boundary condition for ozone.
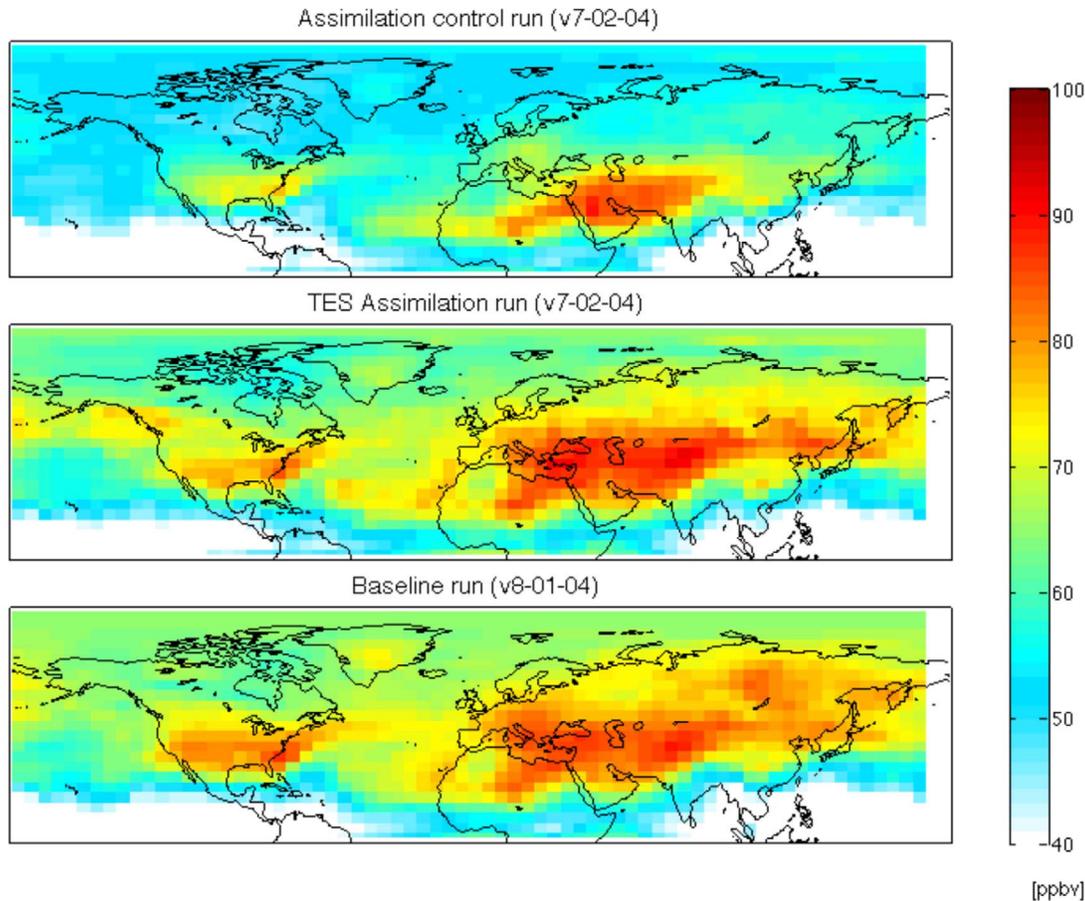
Figure 3. Monthly mean ozone concentrations for July 2006 in the middle troposphere (model level 9, approximately 6 km altitude) (top) for the assimilation control, (middle) for the Tropospheric Emission Spectrometer (TES) assimilation runs in v7-02-04, and (bottom) for the baseline simulation in v8-01-04. The difference between the Figures 3 (top) and 3 (middle) shows the impact of assimilating TES ozone profiles.

[24] As seen in Figure 3, the TES assimilation shows large increases in ozone in the Arctic relative to the assimilation control run, even though no TES data were ingested into the assimilation poleward of 60°N. Figure 4 compares the vertical profiles of ozone from the baseline (green), assimilation (red), and assimilation control (blue) runs at Eureka and Ny-Ålesund in July. The mean model bias below 300 hPa relative to the ozonesondes is reduced from −9.9 ppbv (−16%) in the assimilation control run to −3.5 ppbv (−6%) at Eureka with the TES assimilation, and from −9.4 ppbv (−16%) to −2.4 ppbv (−5%) at Ny-Ålesund. The concentrations near the surface at these two sites show little change with the assimilation. The agreement with the TES assimilation and the ozonesondes in the Arctic suggests that the meteorological fields driving the model (v7-02-04 and v8-01-04) provide an unbiased description of transport into the Arctic.

[25] Figure 3 also demonstrates that the baseline simulation (version 8-01-04 without assimilation) compares well with the TES assimilation. In the middle troposphere of the midlatitudes, between 20°N and 50°N, the mean bias in ozone between the two model simulations is 0.9 ppbv. The high-latitude ozone distribution in the baseline simulation is also consistent with the TES assimilation, as are the ozonesonde observations, as seen in Figure 4. The differences in the mean abundance of ozone in the Arctic summer between the baseline simulation and the TES assimilation are less than 5%. The agreement between the baseline simulation and the TES assimilation in the Arctic suggests that the baseline model is providing a reliable description of transport of midlatitude ozone into the Arctic. This gives us confidence that the tagged ozone analysis presented below gives a meaningful assessment of the impact of the midlatitude source regions on Arctic ozone abundances.

[26] *Parrington et al.* [2008] and *Jourdain et al.* [2010] suggested that the underestimate of ozone in the assimilation control run is due mainly to an underestimate of lightning NO_x (LNO_x) emissions in v7-02-04 of GEOS-Chem. To assess the extent to which the improvements seen in Figure 3 are due to the changes in the LNO_x source, we ran version v8-01-04 of GEOS-Chem with the same surface emissions as in v7-02-04, but kept the OTD-LIS scaling of the LNO_x emissions. This run is labeled "Old emissions" in Table 1. Table 3 shows that the increases in ozone obtained with the TES assimilation relative to the assimilation control run are comparable in the middle (400–750 hPa) and upper
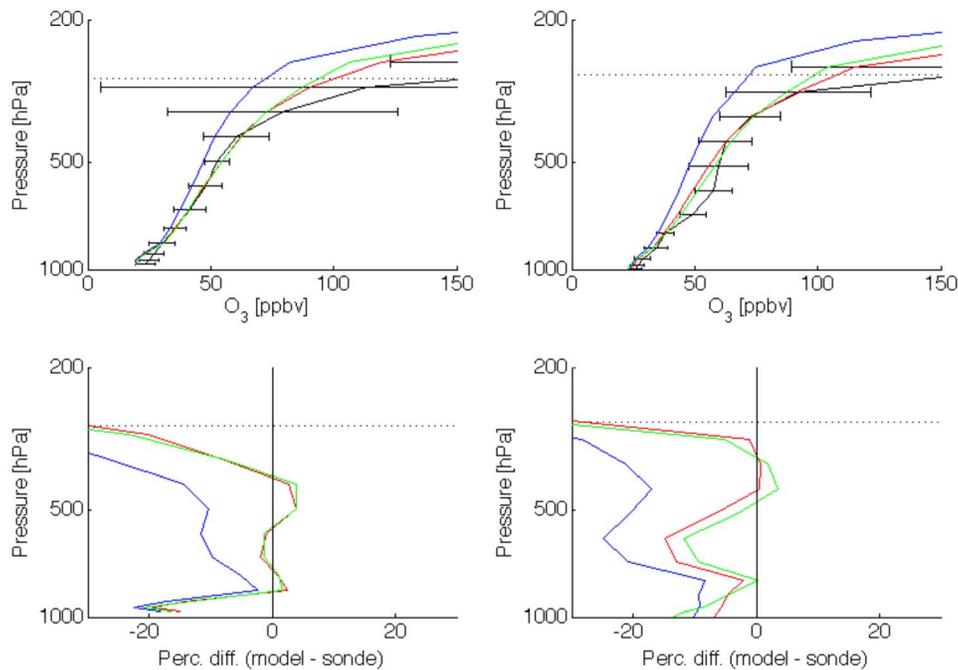
Figure 4. Vertical profiles of mean ozone mixing ratio for July–August 2006 above (left) Eureka and (right) Ny-Ålesund. Ozonesonde observations are shown in black, with error bars showing the standard deviation of the observations. Values from GEOS-Chem v7-02-04 without assimilation are shown in blue (assimilation control simulation). Values from the assimilation run are shown in red, and values from v8-01-04 (baseline simulation) are shown in green. The horizontal dotted black line denotes the mean tropopause pressure for this period.

(above 400 hPa) troposphere to those increases obtained with the improved LNO_x source (the main difference between the old emissions and assimilation control runs). In the middle and upper troposphere the TES assimilation increased ozone by 14% and 33%, respectively, whereas the new LNO_x source enhanced ozone by 19% and 33%, respectively. This suggests that in the free troposphere, the TES assimilation is indeed largely correcting the underestimate in midlatitude ozone due to the lightning precursor emissions in v7-02-04.

3.2. Impact of Midlatitude Continental Source Regions on Arctic Ozone

[27] We conducted a tagged ozone analysis to quantify the contribution of ozone from midlatitude continental source regions to the budget of ozone in the Arctic. In the tagged ozone simulation the ozone chemistry is linearized using production rates and loss frequencies archived from the baseline run. This allows us to use separate tracers to track odd oxygen ($O_x = O_3 + NO_2 + 2NO_3 + PAN + MPAN +$

$PPN + 3N_2O_5 + HNO_4 + HNO_3$) produced in the different source regions shown in Figure 5. The Arctic region shown in Figure 5 includes everything north of 60°N, including parts of northern Canada, Scandinavia, and Russia.

[28] Figures 6 and 7 show the fractional contribution to the simulated ozone distribution above Eureka and Ny-Ålesund, respectively, from the six regions (the stratosphere, Asia, Europe, North America, Siberia, and the Arctic) that represent the dominant contributions to the ozone budget. Transport from other source regions provide contributions of less than 5% and are not examined here. The corresponding total O_x distributions at these sites are shown in Figure 2 (bottom).

[29] The stratospheric tracer has its maximum influence at Eureka in early spring, and its contribution increases with altitude. Little stratospheric influence reaches the surface in the summer and autumn, consistent with Lagrangian studies of stratospheric influence at Arctic surface sites [*Stohl*, 2006; *Hirdman et al.*, 2010]. However, analysis of long-term ozonesonde records in the Arctic show statistically significant correlations in ozone anomalies that link the lower

Table 3. Differences in the Mean Ozone Concentrations North of 60°N in the Lower, Middle, and Upper Troposphere Between Pairs of Forward Model Sensitivity Simulations[a]

Simulations	Arctic LT	Arctic MT	Arctic UT
TES assimilation - assimilation control	1.0 ppbv, 3.6%	6.6 ppbv, 14%	21 ppbv, 33%
Old emissions - assimilation control	2.0 ppbv, 7.1%	9.1 ppbv, 19%	21 ppbv, 33%
TES assimilation - baseline	0.8 ppbv, 3.0%	−2.9 ppbv, −5.1%	−0.1 ppbv, −0.1%
Baseline - no PAN	1.8 ppbv, 6.2%	−1.1 ppbv, −1.9%	−3.4 ppbv, −3.9%

[a]LT, lower troposphere (surface to 750 hPa); MT, middle troposphere (750 to 400 hPa); UT, upper troposphere (400 hPa to tropopause).
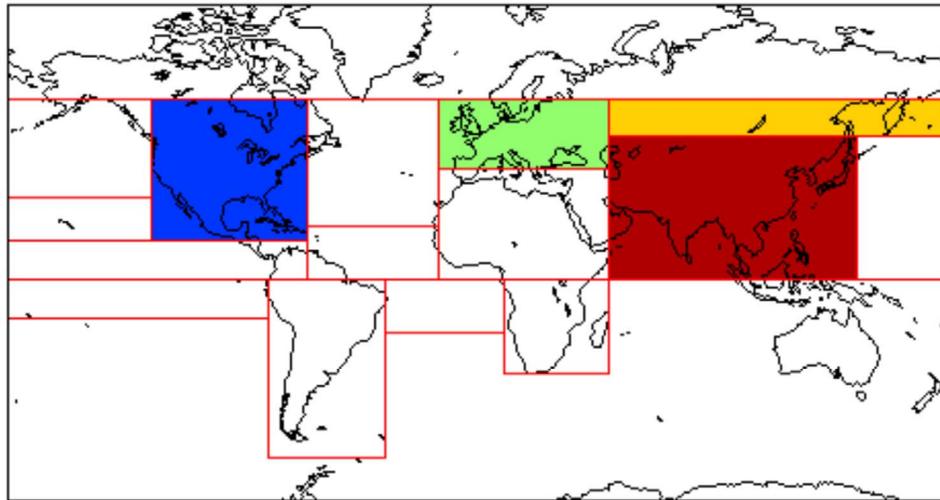
Figure 5. Region definitions for tagged ozone simulation. Midlatitude regions discussed in Figures 6 and 7 are colored. The Arctic region is defined as everything poleward of 60°N.

stratosphere to the troposphere all the way to the surface [*Tarasick et al.*, 2005]. It was suggested by *Terao et al.* [2008] that the correlations in the observational record could reflect variations in large-scale subsidence down into the Arctic lower troposphere.

[30] The European, North American, and Asian contributions maximize in spring and fall when intercontinental transport is most active [*Stohl*, 2001; *Fiore et al.*, 2009]. In summer, transport times to the Arctic are longer, and air transported to the Arctic from midlatitudes will climb along
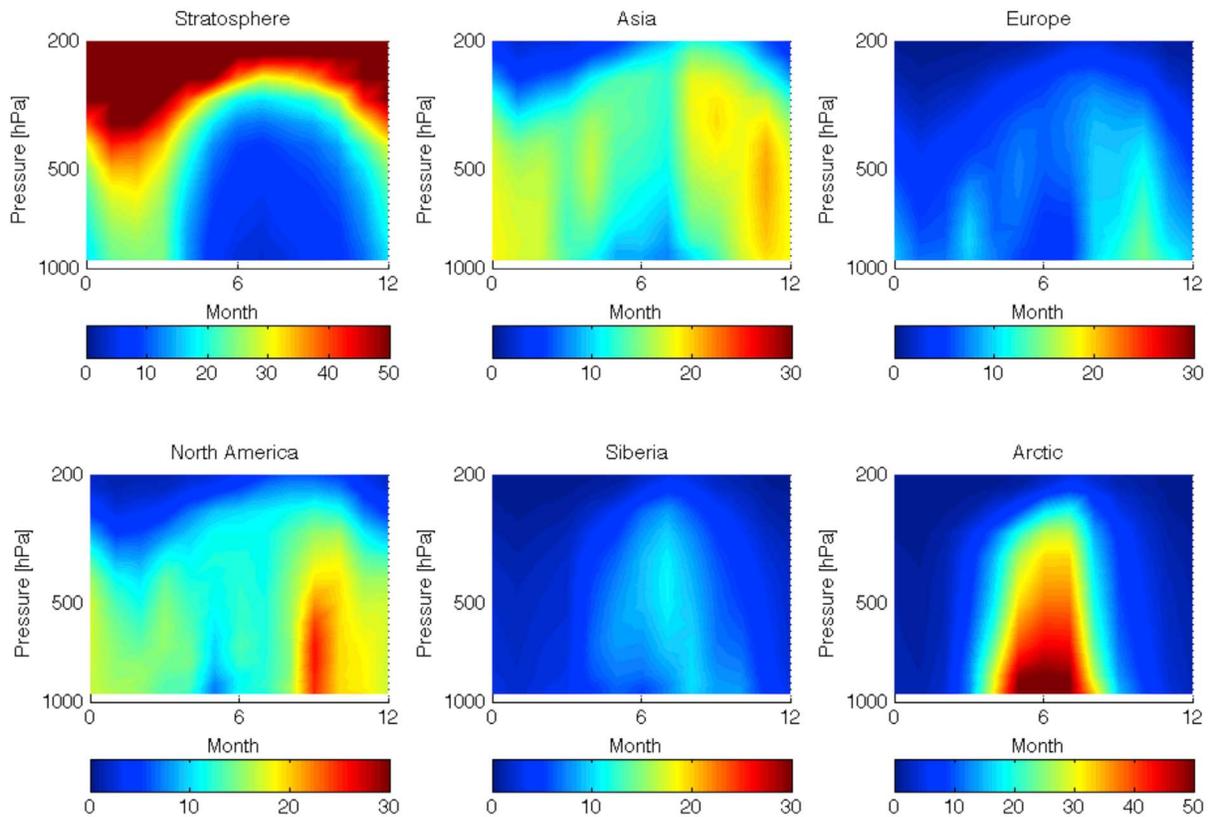

Figure 6. Percent contribution to the ozone profile above Eureka in 2006 due to ozone produced in the stratosphere and in the lower troposphere over Asia, Europe, North America, Siberia, and the Arctic. The contributions were estimated using the tagged ozone simulation, in which separate tracers are specified for ozone produced in each of the source regions shown in Figure 5.
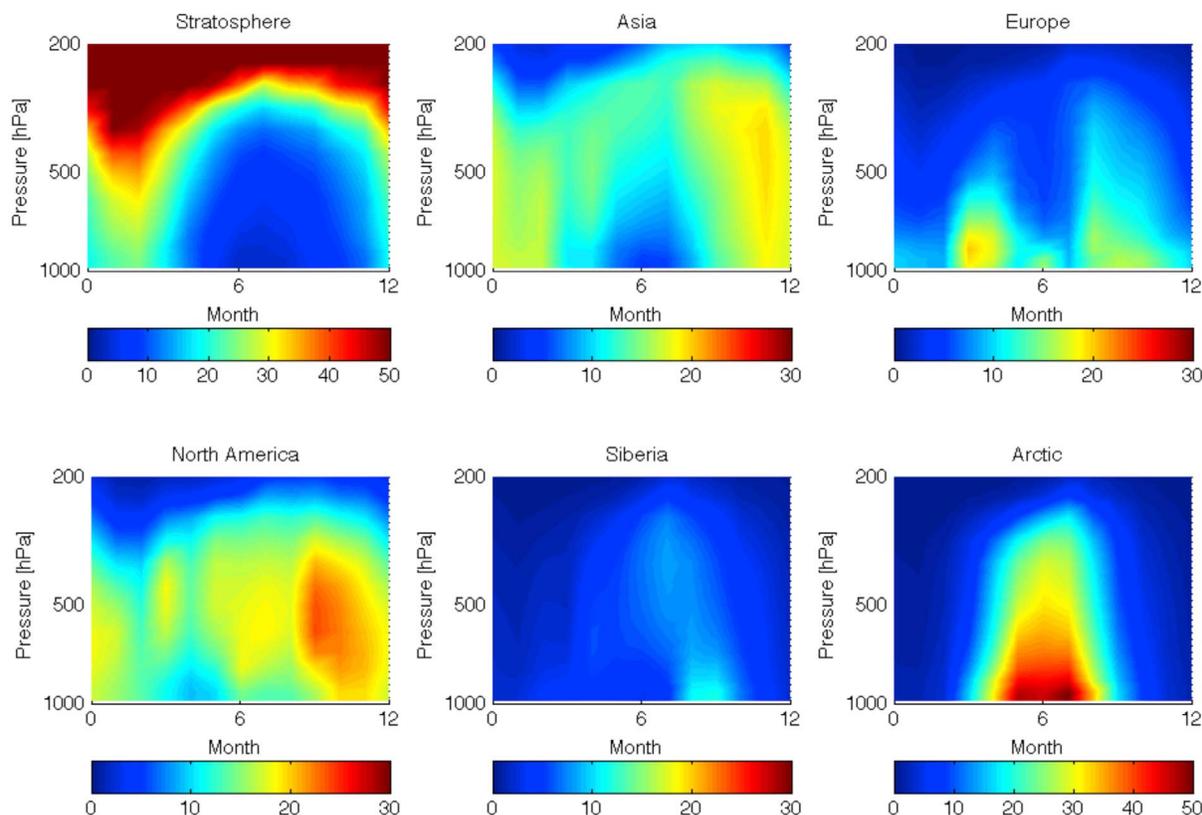
Figure 7. Same as Figure 6, but for the ozone profile above Ny-Ålesund.

isentropic surfaces, effectively isolating the Arctic lower troposphere [*Stohl*, 2006]. As a result, only high-latitude sources in regions such as Siberia, Europe, and North America are expected to have much influence on surface ozone abundances in the Arctic. Pollutants transported from lower latitudes will influence the Arctic at higher altitudes [*Eckhardt et al.*, 2003]. Consequently, we find that the Asian contribution (mainly from East Asia) in the Arctic troposphere in summer is larger in the upper troposphere. Over both Eureka and Ny-Ålesund the Asian contribution is less than 10% throughout the troposphere, but the influence is greater over Eureka than over Ny-Ålesund. *Stohl* [2006] identified three pathways for transport to the lower Arctic troposphere: low-level lateral transport, fast low-level transport followed by ascent in the Arctic, and ascent outside the Arctic followed by lateral transport, then descent inside the Arctic. Emissions from northern source regions such as Europe and from boreal fires have access to the first pathway [*Stohl et al.*, 2007], which can be especially efficient during the positive phase of the North Atlantic Oscillation [*Eckhardt et al.*, 2003; *Stohl et al.*, 2007]. Asian pollutants begin at a higher potential temperature, and so have access mainly to the third pathway which can take 15–20 days.

[31] In summer at Eureka (Figure 6) the European influence is small, less than 8% throughout the troposphere. Transport from North America and local production in the Arctic provide the dominant contributions to local ozone abundances. Over Ny-Ålesund (Figure 7) European sources have a much stronger influence. The North American and European sources each account for about 10%–15% of the

ozone abundances at the surface in summer, with a slightly larger contribution from Europe. The greater European influence at the surface at this site is consistent with previous studies [*Duncan and Bey*, 2004; *Stohl*, 2006]. However, the European contribution is confined to the lower troposphere, whereas the North American influence extends into the middle troposphere.

[32] Ozone produced within the Arctic is limited to the sunlit summer months. At Eureka and Ny-Ålesund this local source accounts for more than 50% of the ozone in the lower troposphere and as much as 30%–40% of the ozone in the middle troposphere. As mentioned above, this production is driven mainly by precursor emissions at high latitudes. Below we use the adjoint of the GEOS-Chem model to examine in greater detail the sensitivity of this local ozone source to emissions of NO_x, a key ozone precursor.

3.3. Sensitivity of Arctic Ozone to NO_x Emissions

[33] The adjoint model of GEOS-Chem is used to calculate the sensitivity of ozone in either the lower or middle troposphere above Alert to monthly mean NO_x emissions. A separate adjoint simulation is performed for the first two weeks of each month between April and August 2006. Sensitivities are calculated for every model grid box, and represent the fractional change that would occur in ozone above Alert for a fractional change in the emissions in a particular grid box. This approach provides rapid, detailed information about which types of emissions and which locations are impacting a particular site at a particular time.
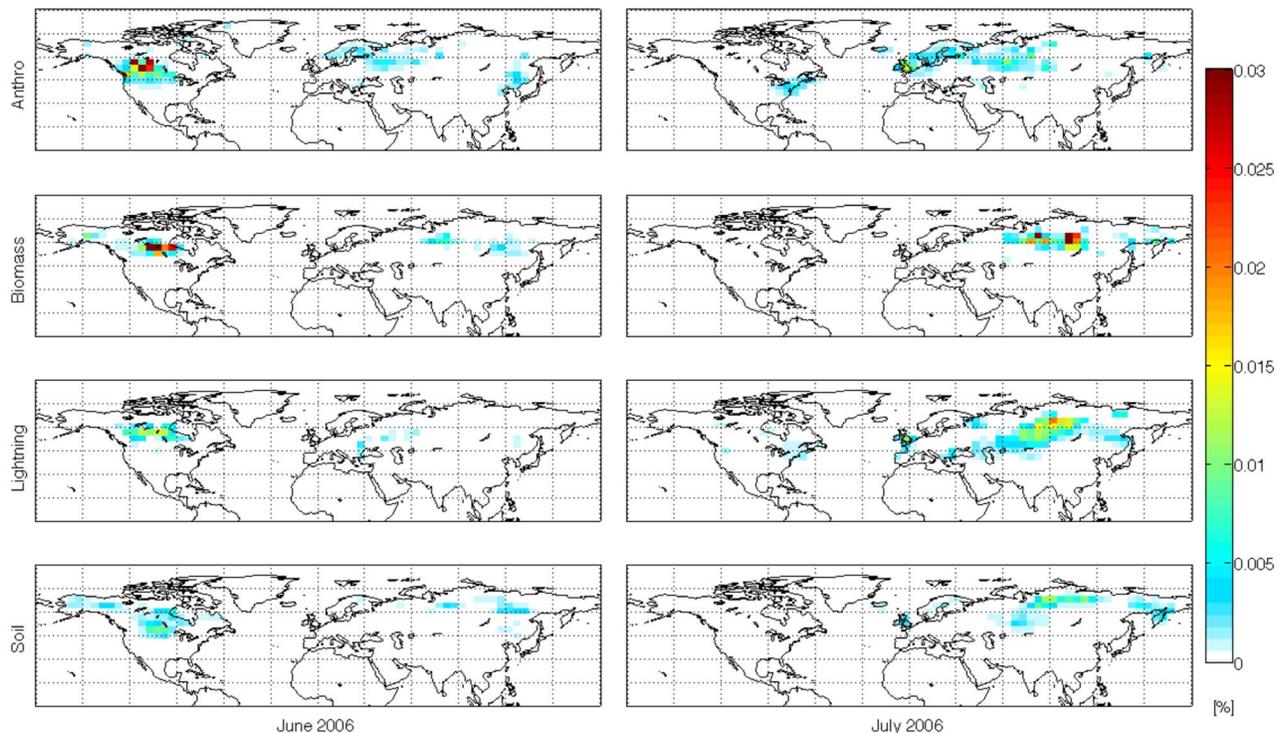
Figure 8. Example maps of the sensitivity of O_x concentration in the middle troposphere above Alert to various types of NO_x emissions. From top to bottom, the plots show the sensitivity to anthropogenic, biomass burning, lightning, and soil NO_x emissions. Sensitivities are shown for the first 2 weeks of (left) June and (right) July of 2006. The color scale indicates the fractional amount by which O_x in the middle troposphere above Alert would change in response to a perturbation in emissions at a particular location.

[34] Figure 8 shows maps of the sensitivities calculated by the adjoint model. Figure 8 (left) shows the sensitivity of ozone in the middle troposphere (850–500 hPa) above Alert to NO_x emissions from fossil fuel combustion, biomass burning, lightning, and from soils in the first two weeks of June 2006. Figure 8 (right) shows the sensitivities in the first two weeks of July 2006. If the sensitivity at a particular location is α, and the emissions at that location were changed by a fractional amount β, then the fractional change in the cost function (here, the O_x abundance in the middle troposphere above Alert) will be $\alpha\beta$. Because the sensitivities reflect the influence of atmospheric transport, the maps depend somewhat on the synoptic conditions during the chosen 2 week simulation period. In the first two weeks of June, North America (mainly western Canada) was the dominant source region for NO_x that influenced ozone abundances over Alert. In particular, ozone over Alert was most sensitive to anthropogenic and biomass burning emissions from northern Alberta. The greatest sensitivity to emissions in Eurasia was to anthropogenic emissions from western Russia and Scandinavia. In contrast, in the first two weeks of July, ozone abundances over Alert were most sensitive to NO_x emissions from biomass burning and lightning in central Russia. There was weaker sensitivity to NO_x emissions from soils in central Russia and from fossil fuel combustion in Scandinavia and the United Kingdom.

[35] To better compare the relative importance of the different sources of NO_x, the zonally summed sensitivities for ozone in the lower and middle troposphere over Alert in the

first two weeks of June, July, and August 2006 are shown in Figure 9. Ozone abundances in the lower troposphere at Alert are most sensitive to NO_x emissions between 55°N and 70°N. Throughout summer there was strong sensitivity to fossil fuel emissions at these latitudes, with comparable sensitivity to soil emissions near 70°N. The sensitivity to biomass burning emissions peaks in July and is comparable to that for fossil fuel emissions near 60°N. In the middle troposphere, ozone was most sensitive to anthropogenic NO_x emissions between 50°N and 60°N, but in July the sensitivity to emissions from lightning and biomass burning increased, and biomass burning emissions near 60°N had the greatest influence on the ozone abundances. By August, the greatest sensitivity in the middle troposphere was to anthropogenic emissions outside the Arctic, between 50°N and 55°N, and to lightning emissions within the Arctic, between 65°N and 70°N.

[36] When interpreting Figures 8 and 9, it is important to note that the sensitivity analysis is only as accurate as the ozone simulation in GEOS-Chem. If our knowledge of the distribution of the ozone precursor emissions is incomplete, or if there are missing processes in the chemical mechanism in the model, the sensitivity analysis will be biased. However, the good agreement between the surface observations and the modeled ozone abundances at Alert suggests that the model is providing a reliable description of the main processes controlling the ozone distribution. Our analysis indicates that on synoptic time scales the local ozone source in the Arctic shown in Figures 6 and 7
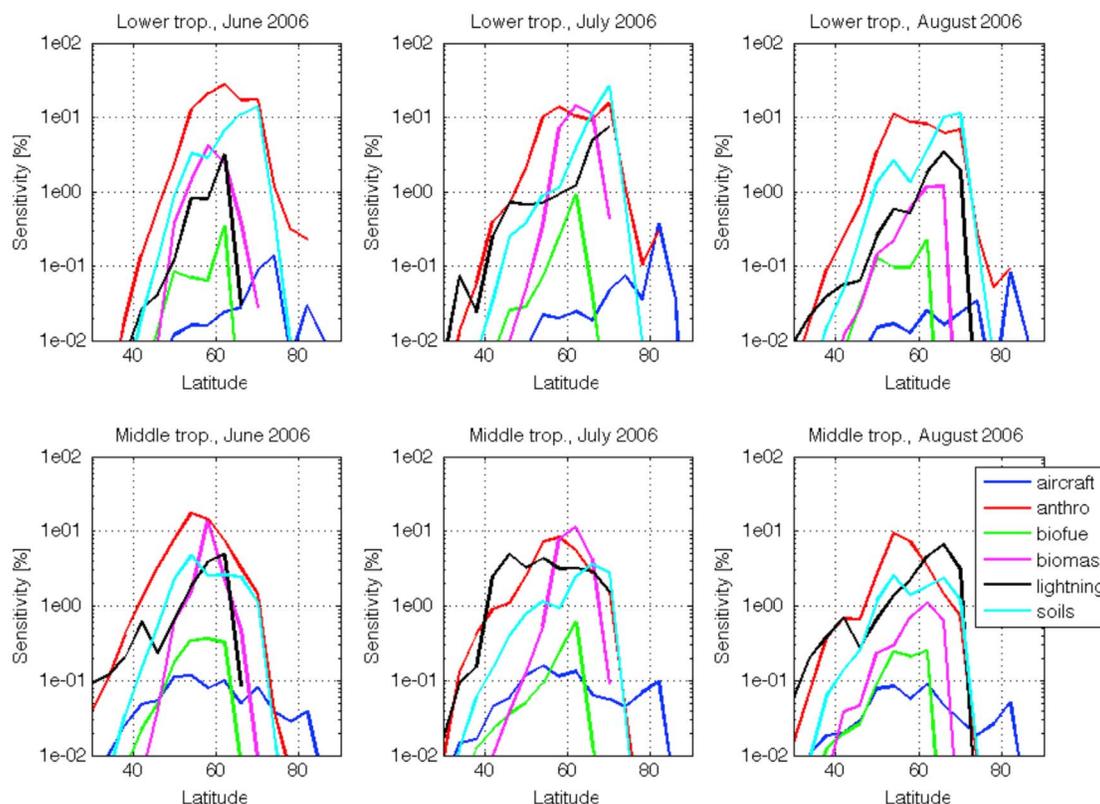
Figure 9. Sensitivity of O_x in percent in the lower (top) and middle (bottom) troposphere above Alert to various sources of NO_x precursor emissions, summed zonally. Sensitivities are shown for the first 2 weeks of June (left), July (middle), and August (bottom) of 2006.

reflects mainly the influence of anthropogenic and soil emissions of NO_x in the Arctic, together with more variable contributions from biomass burning and lightning at high latitudes. On longer time scales, the region to which ozone at Alert is sensitive extends further equatorward, and because different source regions may be included in the region of influence, the relative importance of the different emissions types may change.

3.4. Impact of PAN Decomposition on Ozone Production in the Arctic

[37] Local production of ozone in the Arctic lower troposphere accounts for more than 50% of the ozone budget, but emissions of ozone precursors at high latitudes are small. The release of NO_x from the decomposition of PAN, which acts as a long-lived reservoir for NO_x, is thought to enhance ozone production in the Arctic summer [*Fan et al.*, 1994; *Beine and Krojnes*, 2000]. Long-range transport of PAN from lower latitudes therefore enables the displacement of the ozone-producing capacity of NO_x over long distances [*Singh*, 1987; *Singh et al.*, 1992; *Fan et al.*, 1994]. We examine here the impact of NO_x from PAN decomposition on the ozone budget. We isolate this impact by comparing the baseline run with a simulation of GEOS-Chem with the PAN to NO_x interconversion turned off. Turning off this reaction allows us to separate the influence of this transport pathway (by taking the difference with the baseline run) in a similar way to determining the influence of an emissions source by turning off that emissions source in the model and

comparing to the baseline simulation [*Moxim et al.*, 1996; *Levy et al.*, 1999; *Walker et al.*, 2010].

[38] The baseline simulation gives a good representation of PAN at the surface in the Arctic. Figure 10 shows a year of PAN daily mean mixing ratios measured at Alert in 2001 compared to the values in the baseline simulation. PAN data from this site were only available until 2001, so simulations with emissions appropriate to that year were used for this comparison. PAN concentrations are a minimum in the summer and increase throughout the dark winter. PAN concentrations also fall precipitously from their spring maximum to very low values that persist through the summer, which is consistent with the seasonal cycle observed in the European Arctic [*Beine and Krojnes*, 2000]. Agreement between modeled and observed PAN is good, with a mean model bias in the daily average PAN concentrations of -5.4 pptv (5%).

[39] A number of observations suggest that peroxyacetyl nitrates (PAN + MPAN + PPN) constitute the largest fraction of reactive nitrogen (NO_y) in the Arctic lower troposphere [*Singh*, 1987; *Bottenheim et al.*, 1993] and at higher altitudes as well [*Talbot et al.*, 1994; *Alvarado et al.*, 2010]. Qualitatively, GEOS-Chem reproduces this aspect of the NO_y budget, although recent aircraft observations suggest that the partitioning between nitric acid and PAN in GEOS-Chem is biased [e.g., *Hudman et al.*, 2007; *Walker et al.*, 2010; *Alvarado et al.*, 2010]. *Hudman et al.* [2007] compared the model to aircraft observations of PAN over North America in summer and found that the model reproduced well the data in the lower troposphere, but underestimated
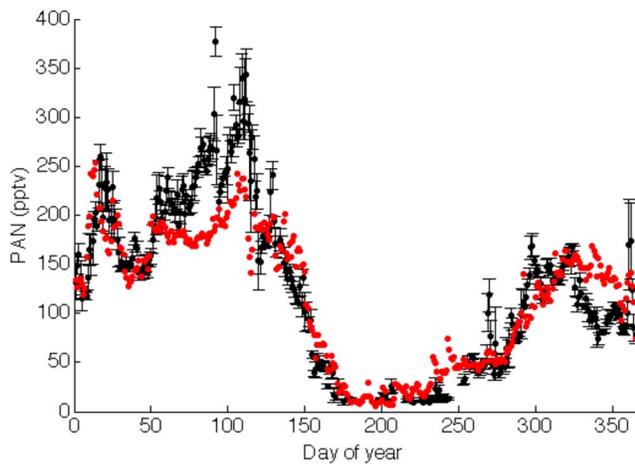
Figure 10. Seasonal cycle of PAN at the surface at Alert (82°N, 62°W) in 2001. Red symbols indicate simulated values from the baseline simulation; black symbols are daily average values of the observations. Vertical error bars represent the standard deviation in the observations over the course of the day.

abundances in the upper troposphere by about 30%. *Alvarado et al.* [2010] examined NO_x and PAN abundances in boreal fire plumes and found that the model PAN accounted for as much as 45% of the NO_y in the fresh plumes, but the model overestimated the HNO_3 to PAN ratio relative to the observations, even after correcting the partitioning at the biomass burning source. *Alvarado et al.* [2010]

suggested that either the simulated emissions of acetaldehyde, an important PAN precursor, are too low, that the biomass burning emissions is injected at too low an altitude in the model, or that the simulated scavenging of nitric acid is underestimated. *Millet et al.* [2010] used remote sensing constraints in GEOS-Chem to estimate a global source of acetaldehyde four times greater than is used here, but with a large uncertainty in the ocean exchange. Nitric acid is often overestimated in global models such as GEOS-Chem, and insufficient scavenging is thought to be the reason [*Bey et al.*, 2001]. However, for the purposes of this study, the ability of the model to reproduce many of the features in the yearlong PAN and ozone observations at Alert lends confidence that the ozone production in the lower troposphere described here does not depend on the exact partitioning of NO_y in the upper troposphere in the model.

[40] Figure 11 (top) shows the zonal mean net production of peroxyacetyl nitrates in May 2006. While the maximum appears at midlatitudes near the surface, the production remains slightly positive in the Arctic midtroposphere. PAN can be cotransported with other species during winter and spring [*Beine and Krojnes*, 2000], or it can be produced in the local Arctic environment from PAN precursors transport from elsewhere. The remote middle troposphere still contains ample precursors to the formation of peroxyacyl radicals, such as acetone [*Brühl et al.*, 2000; *Staudt et al.*, 2003]. We conducted an adjoint sensitivity analysis of the PAN chemistry and found that among peroxyacyl radical precursors, the modeled PAN in the Arctic was most sensitive to acetone abundances. In the model, acetaldehyde levels also persist in the Arctic middle troposphere until April, but
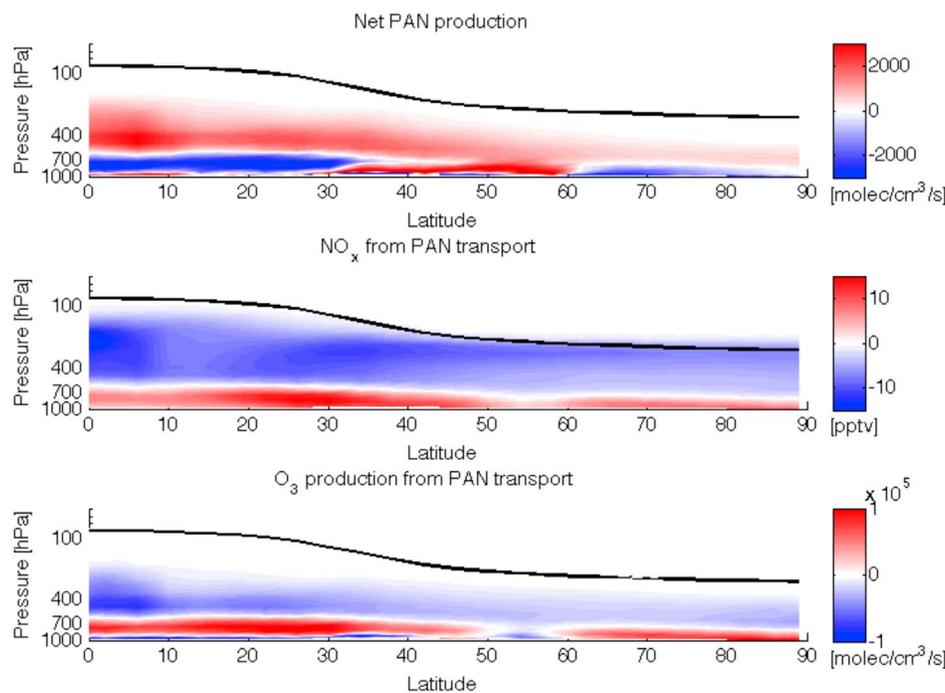

Figure 11. Zonal mean plots during May 2006 of net production of (top) peroxyacetyl nitrates, (middle) the concentration of NO_x due to transport by peroxyacetyl nitrates, and (bottom) ozone production due to transport by peroxyacetyl nitrates. The color bar for net PAN production is saturated in the lower midlatitudes.
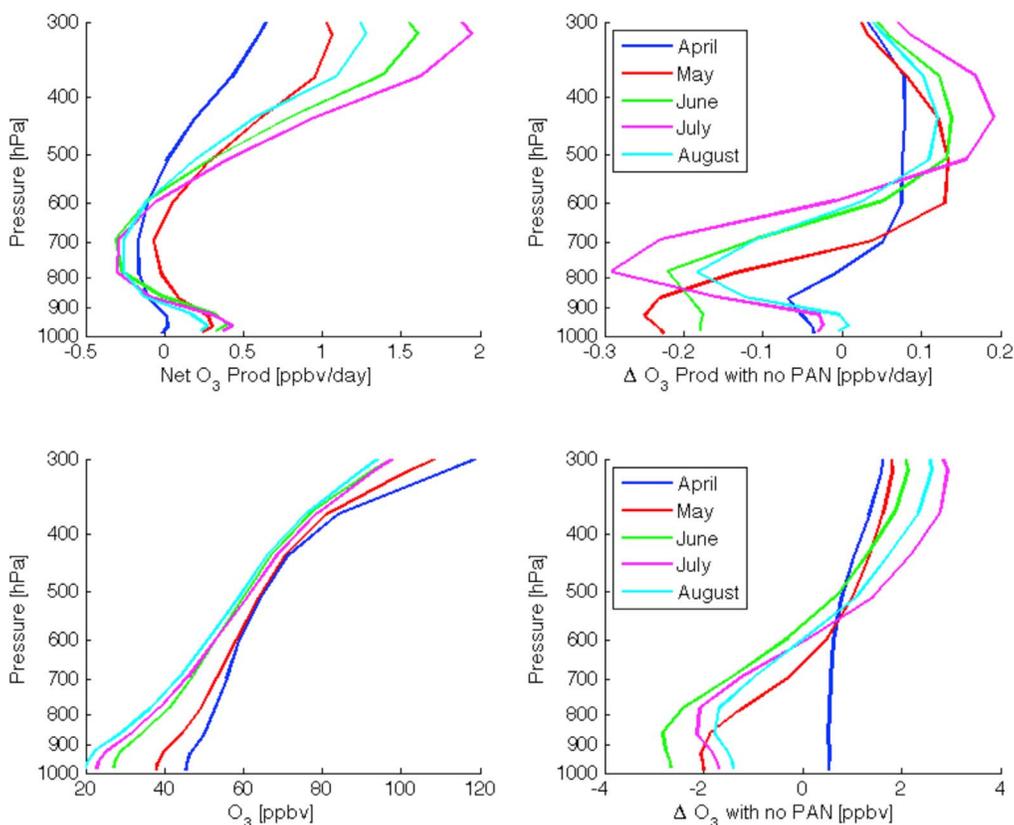
Figure 12. Vertical profiles of (top) net ozone production and (bottom) ozone concentrations averaged north of 60°N for months from April to August 2006. (left) The net ozone production and ozone concentrations from the baseline run and (right) the change in the net ozone production and ozone concentrations as a result of the suppression of the PAN to NO_x interconversion.

are rapidly depleted to mean concentrations of 20 pptv by June, whereas acetone concentrations remain at a background level of about 1 ppbv throughout the summer. The simulation of acetone in this version of GEOS-Chem is known to be biased high; however, the impact of this bias on the PAN concentrations in the Arctic lower troposphere is small and a full discussion of the model acetone budget is beyond the scope of this work.

[41] In the Arctic, the peak in PAN production at around 600 hPa coincides with the peak in organic precursor abundances. Throughout the middle and upper troposphere in the Arctic, PAN production represents a sink for NO_x (Figure 11, middle). On the other hand, the Arctic lower troposphere in May is a region of net PAN destruction, and therefore a source of NO_x and ozone as shown in Figures 11 (middle) and 11 (bottom), respectively.

[42] Ozone produced by locally released NO_x is not static, but evolves through the spring and summer. Figure 12 (left) shows vertical profiles of net ozone production for April through August 2006 in the baseline simulation, averaged across the Arctic. Except in April, the Arctic boundary layer exhibits net production of ozone. As shown in Figure 13, this production is driven by surface NO_x concentrations of about 50 pptv in July. There is also net ozone production throughout spring and summer in the upper troposphere, above 500–600 hPa. In contrast, the lower troposphere between about 850 and 600 hPa, is a net sink for ozone.

This picture of Arctic ozone production is consistent with previous studies [*Fan et al.*, 1994; *Cantrell et al.*, 2003; *Liang et al.*, 2009]. *Liang et al.* [2009] suggested that the increase in NO_x concentrations, and thus the ozone production in the upper troposphere, is driven by transport of NO_x from the stratosphere. However, as shown in Figure 13, we find that emissions of NO_x from lightning provides a significant source of upper tropospheric NO_x.

[43] Figure 12 (right) shows the change in the net ozone production when the reaction that interconverts NO_x and PAN is removed from the chemical mechanism in the model. The changes were obtained by taking the difference of the "no PAN" and baseline simulations. Figure 12 shows that NO_x supplied through PAN was providing up to 0.25 ppbv/d of ozone near the surface in May, when this effect has the greatest impact at the surface. This accounted for 93% of the total ozone production at the surface in May. In June, NO_x from PAN accounted for 55% of the total production at the surface, whereas by August the impact was negligible. In all months in the middle and upper troposphere, above about 600 hPa, suppressing the conversion of NO_x to PAN resulted in a slight increase in net ozone production of about 12%, since PAN production acts as a NO_x sink at these altitudes. Figure 12 (bottom) shows the effect of this chemical pathway on the mean Arctic ozone concentrations. From May to August, NO_x supplied through PAN provides an additional
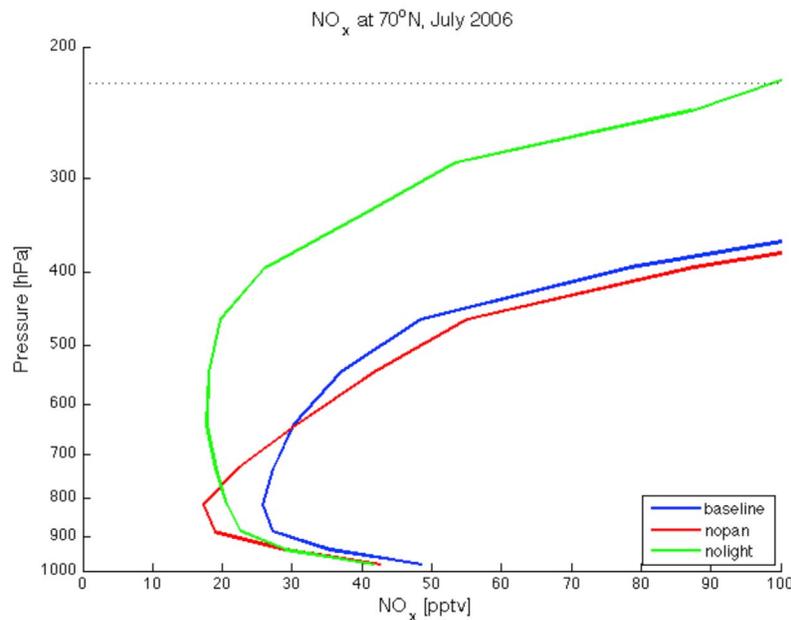
Figure 13. Vertical mean profile of NO_x at 70°N in July 2006. The blue line shows the baseline simulation, the red line shows the "no-PAN" simulation, and the green line shows the baseline simulation with the lightning NO_x source turned off.

2 ppbv of ozone to the Arctic boundary layer, which accounts for up to 10% of the total ozone abundance.

4. Conclusions

[44] We have conducted an analysis of the budget of ozone in the Arctic troposphere in summer 2006 using the GEOS-Chem model. In particular, we focused on quantifying the ozone budget at Eureka, Ny-Ålesund, and Alert, where there are good observational records. When we assimilated TES ozone data to constrain the modeled ozone distribution south of 60°N, the model reproduced well the ozonesonde observations in the Arctic, indicating that the poleward transport of midlatitude ozone in the model is reliable. We found that although the impact of midlatitude emissions on ozone abundances in the Arctic is at a maximum in fall and winter, in July transport from North America, Asia, and Europe together contributed about 25% of surface ozone abundances in the Arctic. As expected, surface ozone abundances at Eureka were influenced more by transport from North America than from Europe, which accounted for 11% and 5% of local surface ozone abundances, respectively. In contrast, at Ny-Ålesund transport of ozone from North America and Europe contributed about 10%–15% each to local ozone abundances. Transport of ozone from Asia had the least impact on the Arctic troposphere. Throughout the summer, the dominant source of ozone in the Arctic troposphere was photochemical production within the Arctic, which accounted for more than 50% of the ozone in the Arctic boundary layer and as much as 30%–40% of the ozone in the middle troposphere.

[45] To better under the processes contributing to summertime ozone abundances in the Arctic, we used the adjoint of GEOS-Chem to perform a sensitivity analysis of the impact of NO_x emissions on ozone at Alert. NO_x is a key ozone precursor and we found that in both the boundary layer and middle troposphere, ozone abundances at Alert were most sensitive to NO_x emissions between 50°N and 70°N. Throughout the summer there was strong sensitivity to anthropogenic emissions at these latitudes, although soil emissions of NO_x in the Arctic, near 70°N, also had a strong influence on surface ozone abundances at Alert. As expected, the influence of biomass burning and lightning was more variable. The sensitivity of middle tropospheric ozone above Alert to lightning emissions at times exceeded that to anthropogenic emissions. In the boundary layer and in the middle troposphere, the sensitivity to biomass burning peaked in the July, when it was comparable to the sensitivity to anthropogenic emissions. We found that in June ozone abundances in the middle troposphere over Alert were most sensitive to anthropogenic and biomass burning emissions from northern Alberta, Canada, whereas in July the greatest sensitivity was to biomass burning and lightning NO_x emissions from Central Russia.

[46] Although local surface emissions of NO_x contributed significantly to ozone production within the Arctic boundary layer, transport of NO_x in the form of PAN from outside the Arctic and from the upper troposphere also contributed to ozone production in the lower troposphere. We found that in late May and June, the release of NO_x from PAN decomposition accounted for 93% and 55%, respectively, of the ozone production at the Arctic surface. By July, the fraction of ozone production at the surface associated with PAN decomposition had decreased to 8%. In the upper troposphere, the production of PAN, which acts as a sink for NO_x, resulted in about a 12% decrease in ozone production, averaged from June through August.

[47] Our results suggest that although the Arctic lower troposphere is more isolated in summer than at other times during the year, transport of ozone from midlatitude source regions does impact surface ozone abundances in the Arctic. An important question that needs to be examined is how climate-related changes in atmospheric transport pathways will influence summertime ozone abundances in the Arctic. There are also climate-related implications for the strong sensitivity that we find in ozone with respect to high-latitude emissions of NO_x from soils and lightning. Although these are natural sources of NO_x, it is important in both an air quality and climate context to understand how changes in climate will influence the contribution of these sources to background ozone levels throughout the Arctic.

References

Alvarado, M. J., et al. (2010), Nitrogen oxides and PAN in plumes from boreal fires during ARCTAS-B and their impact on ozone: An integrated analysis of aircraft and satellite observations, *Atmos. Chem. Phys.*, *10*, 9739–9760.

Beer, R., T. Glavich, and D. Rider (2001), Tropospheric emission spectrometer for the Earth Observing System's Aura satellite, *Appl. Opt.*, *40*, 2356–2367.

Beine, H. J., and T. Krojnes (2000), The seasonal cycle of peroxyacetyl nitrate (PAN) in the European Arctic, *Atmos. Environ.*, *34*, 933–940.

Benkovitz, C. M., M. T. Scholtz, J. Pacyna, L. Tarrasón, J. Dignon, E. C. Voldner, P. A. Spiro, J. A. Logan, and T. E. Graedel (1996), Global gridded inventories of anthropogenic emissions of sulfur and nitrogen, *J. Geophys. Res.*, *101*, 29,239–29,254.

Bey, I., D. J. Jacob, R. M. Yantosca, J. A. Logan, B. D. Field, A. M. Fiore, Q. Li, H. Y. Liu, L. J. Mickley, and M. G. Schultz (2001), Global modeling of tropospheric chemistry with assimilated meteorology: Model description and evaluation, *J. Geophys. Res.*, *106*, 23,073–23,096.

Bottenheim, J. W., L. A. Barrie, and E. Atlas (1993), The partitioning of nitrogen oxides in the lower Arctic troposphere during spring 1988, *J. Atmos. Sci.*, *17*, 15–27.

Bottenheim, J. W., J. D. Fuentes, D. W. Tarasick, and K. G. Anlauf (2002), Ozone in the Arctic lower troposphere during winter and spring 2000 (ALERT2000), *Atmos. Environ.*, *36*, 2535–2544.

Bottenheim, J. W., S. Netcheva, S. Morin, and S. V. Nghiem (2009), Ozone in the boundary layer air over the Arctic Ocean: Measurements during the TARA transpolar drift 2006–2008, *Atmos. Chem. Phys.*, *9*, 4545–4557.

Bowman, K. W., J. Worden, T. Steck, H. M. Worden, S. Clough, and C. Rodgers (2002), Capturing time and vertical variability of tropospheric ozone: A study using TES nadir retrievals, *J. Geophys. Res.*, *107*(D23), 4723, doi:10.1029/2002JD002150.

Bowman, K. W., et al. (2006), Tropospheric Emission Spectrometer: Retrieval method and error analysis, *IEEE Trans. Geosci. Remote Sens.*, *44*(5), 1297–1307.

Boxe, C., et al. (2010), Validation of northern latitude Tropospheric Emission Spectrometer stare ozone profiles with ARC-IONS sondes during ARCTAS: Sensitivity, bias and error analysis, *Atmos. Chem. Phys.*, *10*, 9901–9914.

Brühl, C., U. Pöschl, P. J. Crutzen, and B. Steil (2000), Acetone and PAN in the upper troposphere: Impact on ozone production from aircraft emissions, *Atmos. Environ.*, *34*, 3931–3938.

Cantrell, C. A., et al. (2003), Steady state free radical budgets and ozone photochemistry during TOPSE, *J. Geophys. Res.*, *108*(D4), 8361, doi:10.1029/2002JD002198.

Daescu, D. N., A. Sandu, and G. R. Carmichael (2003), Direct and adjoint sensitivity analysis of chemical kinetic systems with KPP: Part II Numerical validation and applications, *Atmos. Environ.*, *37*, 5097–5114.

Duncan, B. N., and I. Bey (2004), A modeling study of the export pathways of pollution from Europe: Seasonal and interannual variations (1987–1997), *J. Geophys. Res.*, *109*, D08301, doi:10.1029/2003JD004079.

Duncan, B. N., R. V. Martin, A. C. Staudt, R. Yevich, and J. A. Logan (2003), Interannual and seasonal variability of biomass burning emissions constrained by satellite observations, *J. Geophys. Res.*, *108*(D2), 4100, doi:10.1029/2002JD002378.

Eckhardt, S., et al. (2003), The North Atlantic Oscillation controls air pollution transport to the Arctic, *Atmos. Chem. Phys.*, *3*, 1769–1778.

Evans, M. J., and D. J. Jacob (2005), Impact of new laboratory studies of N_2O_5 hydrolysis on global model budgets of tropospheric nitrogen oxides, ozone and OH, *Geophys. Res. Lett.*, *32*, L09813, doi:10.1029/2005GL022469.

Fan, S.-M., and D. J. Jacob (1992), Surface ozone depletion in Arctic spring sustained by bromine reactions on aerosols, *Nature*, *359*, 522–524.

Fan, S.-M., D. J. Jacob, D. L. Mauzerall, J. D. Bradshaw, S. T. Sandholm, D. R. Blake, H. B. Singh, R. W. Talbot, G. L. Gregory, and G. W. Sachse (1994), Origin of tropospheric NO_x over subarctic eastern Canada in summer, *J. Geophys. Res.*, *99*(D8), 16,867–16,877.

Fiore, A. M., D. J. Jacob, I. Bey, R. M. Yantosca, B. D. Field, A. C. Fusco, and J. G. Wilkinson (2002), Background ozone over the United States in summer: Origin, trend, and contribution to pollution episodes, *J. Geophys. Res.*, *107*(D15), 4275, doi:10.1029/2001JD000982.

Fiore, A. M., et al. (2009), Multimodel estimates of intercontinental source-receptor relationships for ozone pollution, *J. Geophys. Res.*, *114*, D04301, doi:10.1029/2008JD010816.

Giering, R., and T. Kaminski (1998), Recipes for adjoint code construction, *ACM Trans. Math. Software*, *24*, 437–474.

Gou, T., and A. Sandu (2011), Continuous versus discrete advection adjoints in chemical data assimilation with CMAQ, *Atmos. Environ.*, *45*, 4868–4881.

Hakami, A., D. K. Henze, J. H. Seinfeld, K. Singh, A. Sandu, S. Kim, D. Byun, and Q. Li (2007), The adjoint of CMAQ, *Environ. Sci. Technol.*, *41*(22), 7807–7818.

Helmig, D., S. J. Oltmans, D. Carlson, J.-F. Lamarque, A. Jones, C. Labuschagne, K. Anlauf, and K. Hayden (2007), A review of surface ozone in the polar regions, *Atmos. Environ.*, *41*, 5138–5161, doi:10.1016/j.atmosenv.2006.09.053.

Henze, D. K., A. Hakami, and J. H. Seinfeld (2007), Development of the adjoint of GEOS-Chem, *Atmos. Chem. Phys.*, *7*, 2413–2433.

Henze, D. K., J. H. Seinfeld, and D. T. Shindell (2009), Inverse modeling and mapping US air quality influences of inorganic $PM_{2.5}$ precursor emissions using the adjoint of GEOS-Chem, *Atmos. Chem. Phys.*, *9*, 5877–5903.

Hirdman, D., et al. (2010), Source identification of short-lived air pollutants in the Arctic using statistical analysis of measurement data and particle dispersion model output, *Atmos. Chem. Phys.*, *10*, 669–693.

Hudman, R. C., et al. (2007), Surface and lightning sources of nitrogen oxides over the United States: Magnitudes, chemical evolution, and outflow, *J. Geophys. Res.*, *112*, D12S05, doi:10.1029/2006JD007912.

Huntrieser, H., et al. (2008), Lightning activity in Brazilian thunderstorms during TROCCINOX: Implications for NO_x production, *Atmos. Chem. Phys.*, *8*, 921–953.

Jacobson, M. Z. (2010), Short-term effects of controlling fossil-fuel soot, biofuel soot and gases, and methane on climate, Arctic ice, and air pollution health, *J. Geophys. Res.*, *115*, D14209, doi:10.1029/2009JD013795.

Jourdain, L., S. S. Kulawik, H. M. Worden, K. E. Pickering, J. Worden, and A. M. Thompson (2010), Lightning NO_x emissions over the USA constrained by TES ozone observations and the GEOS-Chem model, *Atmos. Chem. Phys.*, *10*, 107–119.

Kivi, R., E. Kyrö, T. Turunen, N. R. P. Harris, P. von der Gathen, M. Rex, S. B. Andersen, and I. Wohltmann (2007), Ozonesonde observations in the Arctic during 1989–2003: Ozone variability and trends in the lower stratosphere and free troposphere, *J. Geophys. Res.*, *112*, D08306, doi:10.1029/2006JD007271.

Klonecki, A., P. Hess, L. Emmons, L. Smith, J. Orlando, and D. Blake (2003), Seasonal changes in the transport of pollutants into the Arctic troposphere: Model study, *J. Geophys. Res.*, *108*(D4), 8367, doi:10.1029/2002JD002199.

Koch, D., and J. Hansen (2005), Distant origins of Arctic black carbon: A Goddard Institute for Space Studies ModelE experiment, *J. Geophys. Res.*, *110*, D04204, doi:10.1029/2004JD005296.

Kopacz, M., D. J. Jacob, D. K. Henze, C. L. Heald, D. G. Streets, and Q. Zhiang (2009), A comparison of analytical and adjoint Bayesian inversion methods for constraining Asian sources of CO using satellite (MOPITT) measurements of CO columns, *J. Geophys. Res.*, *114*, D04305, doi:10.1029/2007JD009264.

Kopacz, M., et al. (2010), Global estimates of CO sources with high resolution by adjoint inversion of multiple satellite datasets (MOPITT, AIRS, SCIAMACHY, TES), *Atmos. Chem. Phys.*, *10*, 855–876.

Kuhns, H., E. M. Knipping, and J. M. Vukovich (2005), Development of a United States–Mexico emissions inventory for the Big Bend Regional Aerosol and Visibility Observational (BRAVO) study, *J. Air Waste Manage.*, *55*, 677–692.

Lamarque, J.-F., and P. G. Hess (2003), Model analysis of the temporal and geographical origin of the CO distribution during the TOPSE campaign, *J. Geophys. Res.*, *108*(D4), 8354, doi:10.1029/2002JD002077.

Law, K. S., and A. Stohl (2007), Arctic air pollution: Origins and impacts, *Science*, *315*, 1537–1540.

Levy, H., II, W. J. Moxim, A. A. Klonecki, and P. S. Kasibhatla (1999), Simulated tropospheric NO_x: Its evaluation, global distribution, and individual source contributions, *J. Geophys. Res.*, *104*, 26,279–26,306.

Liang, Q., A. R. Douglass, B. N. Duncan, R. S. Stolarski, and J. C. Witte (2009), The governing processes and timescales of stratosphere-to-troposphere transport and its contribution to ozone in the Arctic troposphere, *Atmos. Chem. Phys.*, *9*, 3011–3025.

Martin, R. V., et al. (2002), Interpretation of TOMS observations of tropical tropospheric ozone with a global model and in situ observations, *J. Geophys. Res.*, *107*(D18), 4351, doi:10.1029/2001JD001480.

Martin, R. V., D. J. Jacob, R. M. Yantosca, M. Chin, and P. Ginoux (2003), Global and regional decreases in tropospheric oxidants from photochemical effects of aerosols, *J. Geophys. Res.*, *108*(D3), 4097, doi:10.1029/2002JD002622.

Martin, R. V., B. Sauvage, I. Folkins, C. E. Sioris, C. Boone, P. Bernath, and J. Ziemke (2007), Space-based constraints on the production of nitric oxide by lightning, *J. Geophys. Res.*, *112*, D09309, doi:10.1029/2006JD007831.

McLinden, C. A., S. C. Olsen, B. J. Hannegan, O. Wild, M. J. Prather, and J. Sundet (2000), Stratospheric ozone in 3-D models: A simple chemistry and the cross-tropopause flux, *J. Geophys. Res.*, *105*(D11), 14,653–14,665.

Millet, D. B., et al. (2010), Global atmospheric budget of acetaldehyde: 3-D model analysis and constraints from in-situ and satellite observations, *Atmos. Chem. Phys.*, *10*, 3405–3425.

Monks, P. S. (2000), A review of the observations and origins of the spring ozone maximum, *Atmos. Environ.*, *34*, 3545–3561.

Moxim, W. J., H. Levy II, and P. S. Kasibhatla (1996), Simulated global tropospheric PAN: Its transport and impact on NO_x, *J. Geophys. Res.*, *101*, 12,621–12,638.

Nassar, R., et al. (2008), Validation of Tropospheric Emission Spectrometer (TES) nadir ozone profiles using ozonesondes measurements, *J. Geophys. Res.*, *113*, D15S17, doi:10.1029/2007JD008819.

Olivier, J. G. J., and J. J. M. Berdowski (2001), Global emissions sources and sinks, in *The Climate System*, edited by J. Berdowski, R. Guicherit, and B. J. Heij, pp. 33–77, Swets and Zeitlinger, Lisse, Netherlands.

Oltmans, S. J., et al. (2006), Long-term changes in tropospheric ozone, *Atmos. Environ.*, *40*, 3156–3173.

Parrington, M., D. B. A. Jones, K. W. Bowman, L. W. Horowitz, A. M. Thompson, D. W. Tarasick, and J. C. Witte (2008), Estimating the summertime tropospheric ozone distribution over North America through assimilation of observations from the Tropospheric Emission Spectrometer, *J. Geophys. Res.*, *113*, D18307, doi:10.1029/2007JD009341.

Parrington, M., D. B. A. Jones, K. W. Bowman, A. M. Thompson, D. W. Tarasick, J. Merrill, S. J. Oltmans, T. Leblanc, J. C. Witte, and D. B. Millet (2009), Impact of the assimilation of ozone from the Tropospheric Emission Spectrometer on surface ozone across North America, *Geophys. Res. Lett.*, *36*, L04802, doi:10.1029/2008GL036935.

Pickering, K. E., Y. Wang, W.-K. Tao, C. Price, and J.-F. Müller (1998), Vertical distributions of lightning NO_x for use in regional and global chemical transport models, *J. Geophys. Res.*, *103*, 31,203–31,216.

Price, C., and D. Rind (1992), A simple lightning parametrization for calculating global lightning distributions, *J. Geophys. Res.*, *97*, 9919–9933.

Quinn, P. K., G. Shaw, E. Andrews, E. G. Dutton, T. Ruoho-Airola, and S. L. Gong (2007), Arctic haze: Current trends and knowledge gaps, *Tellus, Ser. B*, *59*, 99–114.

Quinn, P. K., et al. (2008), Short-lived pollutants in the Arctic: Their climate impact and possible mitigation strategies, *Atmos. Chem. Phys.*, *8*, 1723–1735.

Richards, N. A. D., G. B. Osterman, E. V. Browell, J. W. Hair, M. A. Avery, and Q. Li (2008), Validation of Tropospheric Emission Spectrometer ozone profiles with aircraft observations during the Intercontinental Chemical Transport Experiment-B, *J. Geophys. Res.*, *113*, D16S29, doi:10.1029/2007JD008815.

Sandu, A., D. N. Daescu, and G. R. Carmichael (2003), Direct and adjoint sensitivity analysis of chemical kinetic systems with KPP: Part I Theory and software tools, *Atmos. Environ.*, *37*, 5083–5096.

Sauvage, B., R. V. Martin, A. van Donkelaar, and J. R. Ziemke (2007), Quantification of the factors controlling tropical tropospheric ozone

and the South Atlantic maximum, *J. Geophys. Res.*, *112*, D11309, doi:10.1029/2006JD008008.

Schumann, U., and H. Huntrieser (2007), The global lightning induced nitrous oxides source, *Atmos. Chem. Phys.*, *7*, 3823–3907.

Shindell, D. T., et al. (2008), A multi-model assessment of pollution transport to the Arctic, *Atmos. Chem. Phys.*, *8*, 5353–5372.

Singh, H. B. (1987), Reactive nitrogen in the troposphere—Chemistry and transport of NO_x and PAN, *Environ. Sci. Technol.*, *21*, 320–327.

Singh, H. B., D. Herlth, D. O'Hara, K. Zahnle, J. D. Bradshaw, S. T. Sandholm, R. Talbot, P. J. Crutzen, and M. Kanakidou (1992), Relationship of peroxyacetyl nitrate to active and total odd nitrogen at northern high latitudes: Influence of reservoir species on NO_x and O_3, *J. Geophys. Res.*, *97*, 16,523–16,530.

Singh, K., M. Jardak, A. Sandu, K. Bowman, M. Lee, and D. Jones (2010), Construction of non-diagonal background error covariance matrices for global chemical data assimilation, *Geosci. Model Dev. Discuss.*, *3*, 1783–1827.

Staudt, A. C., D. J. Jacob, F. Ravetta, J. A. Logan, D. Bachiochi, T. N. Krishnamurti, S. Sandholm, B. Ridley, H. B. Singh, and B. Talbot (2003), Sources and chemistry of nitrogen oxides over the tropical Pacific, *J. Geophys. Res.*, *108*(D2), 8239, doi:10.1029/2002JD002139.

Stohl, A. (2001), A 1-year Lagrangian "climatology" of airstreams in the Northern Hemisphere troposphere and lowermost stratosphere, *J. Geophys. Res.*, *106*, 7263–7279.

Stohl, A. (2006), Characteristics of atmospheric transport into the Arctic troposphere, *J. Geophys. Res.*, *111*, D11306, doi:10.1029/2005JD006888.

Stohl, A., et al. (2007), Arctic smoke—Record high air pollution levels in the European Arctic due to agricultural fires in eastern Europe in spring 2006, *Atmos. Chem. Phys.*, *7*, 511–534.

Streets, D. G., et al. (2003), An inventory of gaseous and primary aerosol emissions in Asia in the year 2000, *J. Geophys. Res.*, *108*(D21), 8809, doi:10.1029/2002JD003093.

Streets, D. G., Q. Zhang, L. Wang, K. He, J. Hao, Y. Wu, Y. Tang, and G. R. Carmichael (2006), Revisiting China's CO emissions after TRACE-P: Synthesis of inventories, atmospheric modeling, and observations, *J. Geophys. Res.*, *111*, D14306, doi:10.1029/2006JD007118.

Talbot, R. W., et al. (1994), Summertime distribution and relations of reactive odd nitrogen species and NO_y in the troposphere over Canada, *J. Geophys. Res.*, *99*, 1863–1885.

Tarasick, D. W., V. E. Fioletov, D. I. Wardle, J. B. Kerr, and J. Davies (2005), Changes in the vertical distribution of ozone over Canada from ozonesondes: 1980–2001, *J. Geophys. Res.*, *110*, D02304, doi:10.1029/2004JD004643.

Terao, Y., J. A. Logan, A. R. Douglass, and R. S. Stolarski (2008), Contribution of stratospheric ozone to the interannual variability of tropospheric ozone in the northern extratropics, *J. Geophys. Res.*, *113*, D18309, doi:10.1029/2008JD009854.

van der Werf, G. R., J. T. Randerson, L. Giglio, G. J. Collatz, P. S. Kasibhatla, and A. F. Arellano Jr. (2006), Interannual variability in global biomass burning emissions from 1997 to 2004, *Atmos. Chem. Phys.*, *6*, 3423–3441.

van Donkelaar, A., et al. (2008), Analysis of aircraft and satellite measurements from the Intercontinental Chemical Transport Experiment (INTEX-B) to quantify long-range transport of East Asian sulfur to Canada, *Atmos. Chem. Phys.*, *8*, 2999–3014.

Vestreng, V., and H. Klein (2002), Emission data report to UN-ECE/EMEP: Quality assurance and trend analysis and presentation of WebDab, *MSC-W Status Rep. EMEP/MSC-W Note 1/02*, Norw. Meteorol. Inst., Oslo.

Walker, T. W., et al. (2010), Trans-Pacific transport of reactive nitrogen and ozone to Canada during spring, *Atmos. Chem. Phys.*, *10*, 8353–8372.

Wang, Y., et al. (2003), Springtime photochemistry at northern mid and high latitudes, *J. Geophys. Res.*, *108*(D4), 8358, doi:10.1029/2002JD002227.

Worden, H. M., et al. (2007), Comparisons of Tropospheric Emission Spectrometer (TES) ozone profiles to ozonesondes: Methods and initial results, *J. Geophys. Res.*, *112*, D03309, doi:10.1029/2006JD007258.

Worden, J., S. S. Kulawik, M. W. Shephard, S. A. Clough, H. Worden, K. Bowman, and A. Goldman (2004), Predicted errors of tropospheric emission spectrometer nadir retrievals from spectral window selection, *J. Geophys. Res.*, *109*, D09308, doi:10.1029/2004JD004522.

Worden, J., et al. (2009), Observed vertical distribution of tropospheric ozone during the Asian summertime monsoon, *J. Geophys. Res.*, *114*, D13304, doi:10.1029/2008JD010560.

Zhang, L., et al. (2008), Transpacific transport of ozone pollution and the effect of recent Asian emission increases on air quality in North America: An integrated analysis using satellite, aircraft, ozonesonde, and surface observations, *Atmos. Chem. Phys.*, *8*, 6117–6136.

Zhang, L., D. J. Jacob, M. Kopacz, D. K. Henze, K. Singh, and D. A. Jaffe (2009), Intercontinental source attribution of ozone pollution at western

U.S. sites using an adjoint method, *Geophys. Res. Lett.*, *36*, L11810, doi:10.1029/2009GL037950.

K. Anlauf, J. W. Bottenheim, J. Davies, and D. W. Tarasick, Environment Canada, 4905 Dufferin St., Toronto, ON M3H 5T4, Canada.

K. W. Bowman and J. R. Worden, Jet Propulsion Laboratory, California Institute of Technology, 4800 Oak Grove Dr., Pasadena, CA 91109, USA.

C. C. Carouge and L. T. Murray, School of Engineering and Applied Sciences, Harvard University, Cambridge, MA 02138, USA.

D. K. Henze, Department of Mechanical Engineering, University of Colorado at Boulder, Boulder, CO 80309, USA.

D. B. A. Jones, M. Parrington, and T. W. Walker, Department of Physics, University of Toronto, 60 St George St., Toronto, ON M5S 1A7, Canada. (twalker@atmosp.physics.utoronto.ca)

M. Kopacz, Woodrow Wilson School of Public and International Affairs, Princeton University, Princeton, NJ 08544, USA.

C. Shim, Korea Environment Institute, 290 Jinheungno, 122-706 Seoul, South Korea.

K. Singh, Department of Computer Science, Virginia Polytechnic Institute and State University, Blacksburg, VA 24061, USA.

A. M. Thompson, Department of Meteorology, Pennsylvania State University, University Park, PA 16802, USA.

P. von der Gathen, Research Unit Potsdam, Alfred Wegener Institute for Polar and Marine Research, Telegrafenberg A43, D-14473 Potsdam, Germany.